The Joint Institute for Nuclear Astrophysics — *ASC/Alliances Center for Astrophysical Thermonuclear Flashes*

Flame Evolution During the Deflagration Phase of Type Ia Supernovae

D. M. Townsley[1,2], A. C. Calder[1,3,4], S. M. Asida[5], I. R. Seitenzahl[1,2], F. Peng[1,2,3,6], N. Vladimirova[3], D. Q. Lamb[1,3], and J. Truran[1,2,3,7]

[1]University of Chicago; [2]Joint Institute for Nuclear Astrophysics; [3]ASC Flash Center; [4]SUNY, Stonybrook; [5]Hebrew University, Jerusalem; [6]Caltech; [7]Argonne National Laboratory

The Deflagration Phase of a Type Ia Supernova

A flamelet lit in the runaway convective burning core of a near Chandrasekhar Mass White Dwarf (WD) is subject to strong buouancy effects during the succeeding deflagration. There is good reason to suspect this ignition point to be slightly off-center, leading to a rise so vigorous that it breaks the surface of the WD before burning a significant amount of the WD. We have applied an improved model of the flame and nuclear processing in the WD in order to model the dynamics of the growth and rise of flame bubbles in the WD and apply it here to show how the outcome of the deflagration phase can depend on the location of the ignition point.

Flame, Energy Release and Neutronization Model

Building on earlier work by Khokhlov (1995,2000) and Vladimirova et al. (2006), our flame evolves a progress variable ϕ_C from 0 (fuel) to 1 (carbon consumed) according to the advection-reaction-diffusion equation

$$\partial_t \phi_{\rm C} + \vec{u}\cdot\nabla\phi_{\rm C} = \kappa\nabla^2\phi_{\rm C} + \frac{1}{4\tau}(\phi_{\rm C}-\epsilon)(1-\phi_{\rm C}+\epsilon)\ , \qquad (1)$$

where κ and τ are tuned so that the reaction front propagates at the flame speed and is about 4 zones thick. To represent the further stages of burning we define $\phi_{\rm NSQE}$ (consumption of ^{16}O to material in NSQE) and $\phi_{\rm NSE}$ (conversion of Si to Fe to reach NSE). These are evolved using calbrated relaxion times

$$\dot{\phi}_{NSQE} = (\phi_{\rm C}-\phi_{\rm NSQE})/\tau_{\rm NSQE}(T_f)\ , \qquad \dot{\phi}_{NSE} = (\phi_{\rm NSQE}-\phi_{\rm NSE})/\tau_{\rm NSE}(T_f)\ , \qquad (2)$$

where T_f is estimated by predicting the final NSE state for an isobaric burn and $\dot{X}$ represents a Lagrangian derivative. The physical variables are the electron number per baryon, Y_e, the number of nuclei per baryon, Y_i, and the average binding energy per baryon, $\bar{q}$. These evolve via,

$$\dot{\bar{q}} = \dot{\phi}_{\rm C}X^0_{\rm C}(q_{\rm Mg}-q_{\rm C}) + \dot{\phi}_{\rm NSQE}\left\{q_f - \left[(1-X^0_{\rm C})q_{\rm O} + X^0_{\rm C}q_{\rm Mg}\right]\right\} + \phi_{\rm NSQE}\frac{\bar{q}_f-\bar{q}_{\rm ash}}{\tau_{\rm NSQE}(T_f)}\ , \qquad (3)$$

where $\bar{q}_{\rm ash}$ is defined by

$$\bar{q} = X^0_{\rm C}q_{\rm C} + (1-X^0_{\rm C})q_{\rm O} + \phi_{\rm C}X^0_{\rm C}(q_{\rm Mg}-q_{\rm C}) + \phi_{\rm NSQE}\left\{\bar{q}_{\rm ash} - \left[X^0_{\rm C}q_{\rm Mg} + (1-X^0_{\rm C})q_{\rm O}\right]\right\}\ , \qquad (4)$$

and the initial ^{12}C fraction is denoted by $X^0_{\rm C}$ and $\bar{q}_f$ is the estimate for the final NSE state based on burning the current material fully to NSE found by solving $\mathcal{H}-\bar{q} = \mathcal{H}(T_f) - \bar{q}_{\rm NSE}(T_f)$, where $\mathcal{H}$ is the enthalpy per unit mass. Y_i is treated in a similar fashion to $\bar{q}$. Weak processes (e.g. electron capture) are included in the calculation of the energy input rate,

$$\epsilon_{\rm nuc} = \dot{\bar{q}} - \phi_{\rm NSE}[\dot{Y}_{e,f}N_Ac^2(m_p+m_e-m_n) + \epsilon_\nu]\ , \qquad (5)$$

where $\dot{Y}_{e,f}$ and the neutrino loss, ϵ_ν, are calculated by convolving the NSE distribution with the weak interaction cross sections, and $\dot{Y}_e = \phi_{\rm NSE}\dot{Y}_{e,f}$.

Elimination of Noise in Flame

The noise generated by the model flame may influence the outcome of a deflagration simulation by seeding spurious fluid instabilities. Quantifying noise, determining the sources of noise, and minimizing noise are therefore necessary steps in the development of a robust flame model. To this end, we performed a suite of simple test simulations of propagating flames and measured the RMS deviation of the velocity and pressure fields in the fuel, $\sqrt{\langle x^2\rangle - \langle x\rangle^2}$. The simulations presented here are for the "sharpened" KPP shown above with $\epsilon = 10^{-3}$, the highest values for which the RMS deviation in velocity was a limited to a few$\times 10^{-4}$. Simulations of model flames utilizing the "top hat" reaction produced considerably more noise, ~ 0.1 or more RMS velocity deviation.

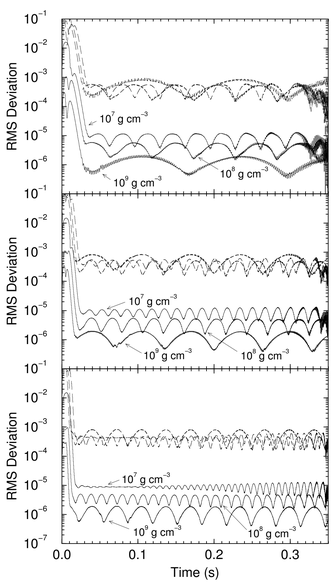

Figure 3: Shown are the RMS velocity (dashed) and pressure (solid) deviation in the fuel preceding a steady-state propagating flame in one dimension in which the ash is at rest. These are all for a flame speed of 60 km s^{-1} and resolutions of 0.16, 0.08 and 0.04 km, and various densities are shown. All these tests use the full energetics implementation. The dominant noise features are due to the initial transient, whose length varies with resolution because it is related to the flame self-crossing time, and the regular periodic feature due to the noise emitted as the flame front propagates through the domain, which shows a period of $c_s\Delta x/(s\rho_{\rm fuel}/\rho_{\rm ash})^2$.

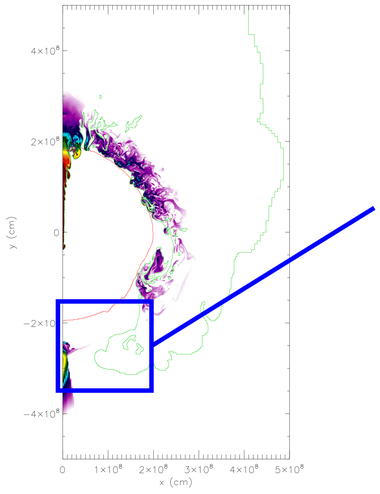

Figure 1: Evolution of the collision region from collision to detonation for a deflagration started with an ignited bubble of radius 16 km offset 40 km from the stellar center in the upward direction. Temperature is indicated by color and contours show the edge of the burned material ($\phi_{\rm C} = 0.1$, green) and density of 10^7 g cm^{-3} (red). This is an example of the gavitaniotally confined detonation (GCD; Plewa, Calder, & Lamb 2004) process. The breakout of the hot, expanding material drives a surface flow of gravitationally bound material toward the opposite pole. As shown, we find that the colliding material forms a compression region that creates both an outward and inward(upward)-directed jet-like structure. The detonating material then appears to be inertially confined at the WD surface by this flow originating at the collision point, although the amount of compression occuring likely reflects both the strongly gravitationally stratified WD surface and a certain amount of assistance from gravity, such that both high gravity and and a flow with significant inertia are required to reach such high temperatures and densities. The kinetic motion imparted to the material by the expanding bubble at the breakout point leads to the eventual (gravitationally assisted) confinement.

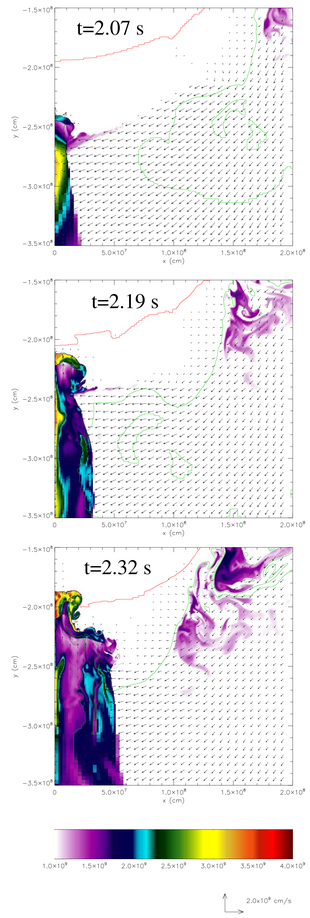

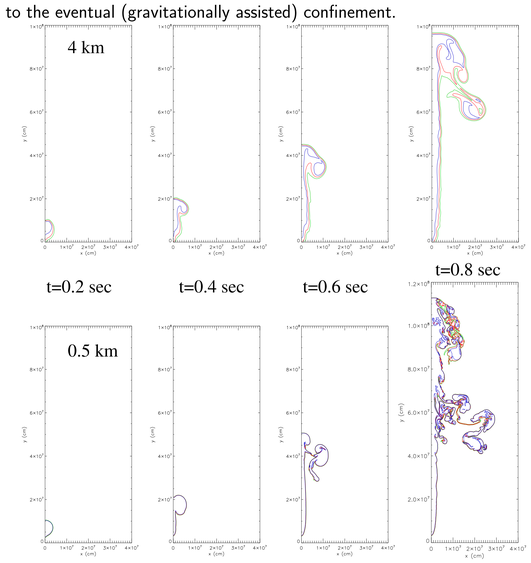

Figure 2: Stages of bubble growth at different resolution for initial bubble of radius 16 km offset 40 km from the center of the star. Shown are contours of $\phi_{\rm C} = 0.1$ (green), 0.5 (red) and 0.9 (blue). We distinguish three stages of evolution in terms of the critical wavelength $\lambda_c \simeq 4\pi s^2/Ag$ (Khokhlov 1995) for the Raleigh-Taylor instability to significantly perturb the flame surface. here s is the flame speed and $A = (\rho_{\rm fuel}-\rho_{\rm ash})/(\rho_{\rm fuel}+\rho_{\rm ash})$ and g is gravity. (1) laminar bubble growth where $r_{\rm bub} < \lambda_c$, the critical wavelength for R-T turnover, which appears in the leftmost panel. (2) Resolved R-T, which begins when $r_{\rm bub} \simeq \lambda_c$ with the first roll as seen in the second panel and continues in the third panel for the finer resolution. (3) Unresolved R-T in which λ_c is smaller than the resolution, which both simulations eventually transition into.

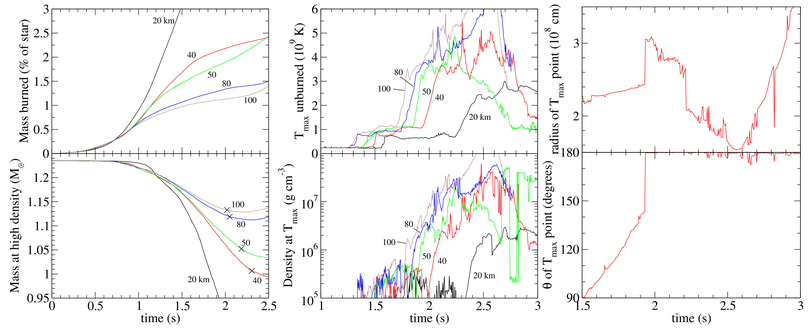

Figure 4: Evolution with time during the deflagration phase for a variety of central offsets of the ignition region. All simulations at 4 km resolution. First panel: burned mass (as a fraction of the star) and mass with $\rho > 5.5\times10^7$ g cm^{-3}. The point at which conservative detonation criteria ($T > 3\times10^9$ K, $\rho > 10^7$ g cm^{-3}) are reached are marked with $\times$. Second Panel: Maximum temperature in the unburned material in the lower hemisphere and the density at the same point. Third Panel: Location of the maximum temperature point in radius and polar angle for the case with $r_{\rm off} = 40$ km. The stellar surface is at approximately 2×10^8 cm.

Variation of Outcomes from Initial Conditions

We find that the mass of the star at high densities and therefore the amount of ^{56}Ni expected in the ejecta is correlated with the offset of the initial (small) ignition region. Larger offsets can produce more ^{56}Ni for two reasons: (1) less energy is released in the deflagration phase, and therefore the star has expanded less when the detonation occurs, and (2) the detonation conditions happen sooner so that the star has had less time to expand. It does appear that the first of these is the dominant effect. The top panel of Figure ?? shows the mass burned as a fraction of the star with time. Larger offsets burn less of the star during the bubble rise and breakout, leading to less expansion of the star.

Resolution Study

Some properties of the off-center deflagration model that we are trying to deduce from our simulations show dependence on the simulation resolution, while others do not. We would like to make statements as much as possible based on features that are not influenced by resolution, and where we cannot avoid it, account for the dependence in other conclusions that we draw. Problems with resolution-dependence is not entirely unexpected, since a significant amount of our simulation is *a priori* known to be unresolved. We find that the conditions at the possible detonation point are fairly insensitive to resolution, for the resolutions considered, but that the state of the interior of the star at a given time during the runaway may only be calculated by higher resolution simulations than the 4 km at which our parameter study was performed.

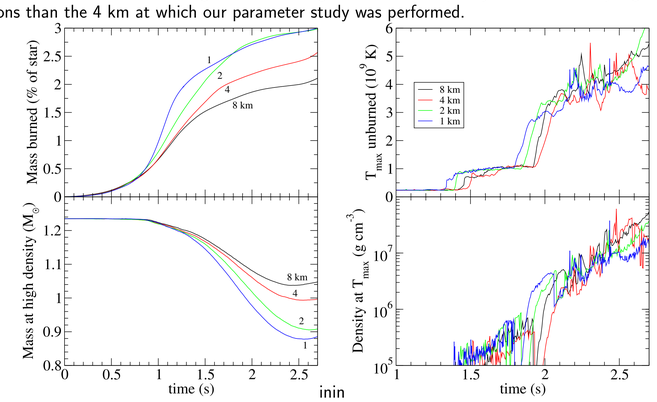

Figure 5: Evolution during the deflagration phase for the same ignition condition, $r_{\rm bub} = 16$ km, $r_{\rm off} = 40$ km, for various resolutions between 8 and 1 km. See figure 4 above for a description of the quantities shown. Integral stellar quantities shown on the left have a noticeable dependence on resolution, though our finest resolutions are consistent. The conditions at the collision point, however, show little dependence on resolution.

References

Khokhlov, A. M. 1995, ApJ, 449, 695

Khokhlov, A. M. 2000, astro-ph/0008463

Plewa, T., Calder, A. C., & Lamb, D. Q. 2004, ApJ, 612, L37

Vladimirova, N., Weirs, G., & Ryzhik, L. 2006, Combust. Theory Modelling, 10, 727

This work is supported under NSF Grant PHY 02-16783 to the Joint Institute for Nuclear Astrophysics, an NSF Physics Frontier Center and by the Department of Energy under contract B523820 to the Center for Astrophysical Thermonuclear Flashes at the University of Chicago.